8-2011

A Two-Dimensional Numerical Simulation of Plasma Wake Structure Around a CubeSat

Rajendra Mitharwal
Utah State University

A TWO-DIMENSIONAL NUMERICAL SIMULATION OF PLASMA WAKE STRUCTURE AROUND A CUBESAT

by

Rajendra Mitharwal

A thesis submitted in partial fulfillment
of the requirements for the degree

of

MASTER OF SCIENCE

in

Electrical Engineering

Approved:

Dr. Reyhan Baktur Major Professor	Dr. Charles M. Swenson Committee Member
Dr. Bedri A. Cetiner Committee Member	Dr. Mark R. McLellan Vice President for Research and Dean of the School of Graduate Studies

UTAH STATE UNIVERSITY
Logan, Utah

2011

Abstract

A Two-Dimensional Numerical Simulation of Plasma Wake Structure Around a CubeSat

by

Rajendra Mitharwal, Master of Science

Utah State University, 2011

Major Professor: Dr. Reyhan Baktur
Department: Electrical and Computer Engineering

A numerical model was developed to understand the time evolution of a wake structure around a CubeSat moving in a plasma with transonic speed. A cubeSat operates in the F2 layer of ionosphere with an altitude of $300 - 600$ Km. The average plasma density varies between $10^{-6}\text{cm}^{-3} - 10^{-9}\text{cm}^{-3}$ and the temperature of ions and electrons is found between $0.1 - 0.2$ eV. The study of a wake structure can provide insights for its effects on the measurements obtained from space instruments. The CubeSat is modeled to have a metal surface, which is a realistic assumption, with a negative electric potential. To solve the equations of plasma, the numerical difference equations were obtained by discretizing the fluid equations of the plasma along with nonlinear Poisson's equation. The electrons were assumed to follow the Boltzmann's relation and the dynamics of ions was followed using the fluid equations. The initial and boundary conditions for the evolution of the structure are discussed. The computation was compared to the analytical solution for a 1D problem before being applied to the 2D model. There was a good agreement between the numerical and analytical solution. In the 2D simulation, we observe the formation of plasma wake structure around the CubeSat. The plasma wake structure consists of rarefaction region where ion density and ion velocity decreases compared to the initial density and velocity.

(47 pages)

I dedicate this to my brother, Virender Mitharwal.

Acknowledgments

I express my gratitude towards my major professor, Dr. Reyhan Baktur, for providing the opportunity to work on a topic which interests me and also providing the support throughout my master's program. This thesis is possible because of her knowledge, guidance, feedback, and review.

I would like to thank Dr. Charles Swenson for guiding me throughout this work, especially when the project seemed far from being possible. His knowledge in both plasma physics and computational science had a tremendous effect on the way I completed this work. I would also like to thank Dr. Bedri Cetiner for his guidance and support. His knowledge in the field of microwaves has always inspired me as a researcher. I would like to acknowledge Dr. Edmund Spencer for his inspiration. His teachings on space physics, fluid dynamics, and partial differential equations led me to develop the necessary theoretical background in the least possible time. I would also like to thank my graduate student advisor, Mary Lee Anderson, for proofreading this thesis and her help throughout the graduate work.

I love and respect my parents for giving me full support and having faith in me. It's my dad who has instilled in me the importance of mathematics. I express my love for Kabbu for having full faith, trust, and being the source of both inspiration and encouragement.

Rajendra Mitharwal

Contents

List of Figures

Chapter 1

Introduction

The concept of CubeSat began as a collaboration between academic universities to build a deeper understanding of space without big budgets for space missions. A one unit (1U) CubeSat is a small satellite, with a dimension of 10cm x 10cm x 10cm as shown in Fig. 1.1 [1] and weight generally does not exceed 1Kg. The use of standardization in the deployment programs defines the size requirement of a CubeSat [1]. In particular, the use of Poly-Picosatellite Orbital Deployer or the P-PODs [2] which are used in the launch and deployment of CubeSats. The P-POD has a size of three 1U CubeSats. It can accommodate CubeSats of 1U, 1.5U, 2U, and 3U size specifications. The other specifications which affect the design of CubeSats are the size of commercial-off-the-shelf (COTS) components (solar cell and battery), launch vehicle environmental and operational requirement and the safety standards [3].

The development process of CubeSats consists of requirement planning, design analysis, fabrication, quality control, system level testing, integration, launch, and ground-based satellite operations. The standardization across these processes is core to the features of CubeSat Program. It helps in reducing both the mission cost and the development time. The usual time required for the development and deployment is two years. This has caused a growing interest of the student community in the CubeSat programs. CubeSats give the students an opportunity to learn multi-disciplines, which in turn has made the space technology more accessible to academia [3].

There has been varied interest in launching the CubeSat. The most common of them is the enhancement of technology in terms of costs. This includes COTS components, sensors, solar array and antennas [4], tethered systems, and wireless systems. The Earth imaging is an example where these interests has enhanced the technology, particularly the

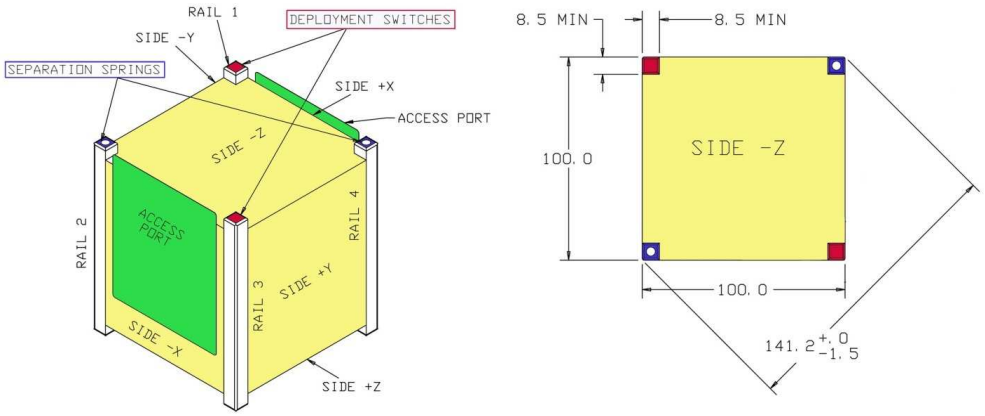

Fig. 1.1: CubeSat.

CMOS camera technology and altitude determination algorithms. These objectives should help in improving our knowledge base of the science involved in space. This includes the understanding of the environment in space and how it affects the Earth (there have been missions to understand earthquakes). The CubeSats orbit in the F2-layer of ionosphere at a speed of $7500 - 7800$ m/s. The characteristics of the plasma found in this region is explained in the next section.

There have been many instances where CubeSats have failed to achieve the science objectives [5]. This necessitates that the steps during design and analysis should be carried with more time on validation and testing. The failure rate can be reduced if there are more testing tools available. Since the CubeSat has to work in space and its difficult to have the same environment conditions on Earth, the computer simulation is the way to learn the working of CubeSat. These simulations have their own advantages with respect to cost and risks. Our work has been in this direction about how the space environment around a CubeSat behaves which can be a valuable data for instrumentation engineers during the design phase. Our simulation aims at understanding the dynamics in formation of wake structure around a CubeSat, when it is placed in the orbit. This understanding becomes important when we want to know whether the spacecraft instruments on board are measuring the plasma properties or the disturbance created by the spacecraft itself. So, the ultimate scientific goal behind our work with these simulations is the validation of the

measurements obtained from the spacecraft instruments.

In our study, we solve the problem in both 1D and 2D. In 1D case, the CubeSat is modeled to be an infinite long metal sheet placed at the origin. In 2D case, the CubeSat is modeled with a 2D square region moving at transonic speed and placed inside the computational domain filled with plasma. The 1D case describes the basic phenomenon of the formation of plasma sheath over an infinite metal surface. The sheath is formed because of the high mobility of the electrons due to which they are easily diffused into the metal wall compared to the ions. The ions accumulate around the metal surface to shield the effect produced by the negative electric potential. The potential varies continuously from the electric potential applied on metal surface to the plasma potential in the region. The simulation starts with the zero initial velocity but achieves the minimum ion velocity required at pre-sheath region [6]. Plasma fluid equations are used to track the ion dynamics, where as Boltzmann's relation is used for electrons. In our work, we use the collisionless, unmagnetized, and nonlinear model of the ideal plasma (two species of the charged particles) described by fluid equations for the isothermal ions and electrons. For 1D case, there are analytical solutions available [7] with which we compare our results. The simulation is run longer enough to achieve the steady state where there is no change in the wake structure.

1.1 CubeSat Environment

A CubeSat operates in the F2 layer of ionosphere with the altitude range in 300-600 Km which is also known as Low Earth Orbits (LEO). They also operate at the range of 200 Km, where the wake structure becomes more important because of the presence of the neutral atoms. These neutral atoms are not absorbed by the satellite surface and this causes an increase in the neutral density on the front surface. The space environment at that altitude is very complex and dynamic. The local satellite environment mainly consists of plasma which is explained in next section. The presence of plasma in this region causes the most common effect known as spacecraft charging. This effect is being seen in the case of the spacecraft instruments, especially Langmuir probes, and is one of the reasons to study the wake structure [8]. It is caused due to the electron influx causing an electric potential

to develop on the satellite. Sometimes the electron flux can cause damage to the circuitry and the electronic systems. The charging of satellite is also caused due to the presence of current flow from the plasma and occasionally due to the emission of photoelectrons from the surface. There are many ways by which spacecraft charging can be reduced. Shielding being one of them, or maintain the spacecraft ground at the plasma potential to stop the flow of current. The newest method to reduce the charging effects is ejection of electron beam out of the spacecraft. There are various effects that take place in this region [9] which are solar ultraviolet (UV) radiation, ionizing radiation, atomic oxygen, and pressure related effects due to presence of high vacuum. They cause mostly the surface degradation of the material used on the CubeSats. In F2 layer, the ionization maximum takes place causing a balance between plasma transport and chemical ion processes. The species of ions found in this region is O+. The ion density varies from $10^{-6}\text{cm}^{-3} - 10^{-9}\text{cm}^{-3}$ [10]. The ion and electron temperature varies from 0.1-0.2 eV [11]. For our simulation, we use 0.1 eV for both electron and ion temperature.

1.2 Plasma

Plasma is a collection of ions, electrons, and neutral atoms formed due to process of ionization. It differs from the ionized gas in the sense that if we consider a small volume, small enough that there is no variation of plasma properties, and big enough that it has large number of particles in it, it shows collective behavior [7]. The charge neutrality is one such collective behavior. Due to its collective nature, plasma can be explained with the help of fluid transport equations explained later in this section. Any plasma is described using Debye length and plasma frequency. The Debye length λ_d is given by

$$\lambda_d = \left(\frac{\epsilon_0 KT}{n_0 e^2}\right), \tag{1.1}$$

where T is the temperature of the charge particles and n_0 is the ambient charge particle density of a neutral plasma. The λ_d determines the distance where the charge imbalance can penetrate for a given disturbance. It also defines the shielding length, the distance where

impact of the external electric field can be observed. In our simulation, when a conducting metal surface is place in the plasma, the so called charge imbalance, also known as plasma sheath, is formed around it and its thickness is of the order of λ_d. The angular frequency also known as plasma frequency is given by

$$\omega_p = \left(\frac{n_0 e^2}{m_e \epsilon_0} \right), \tag{1.2}$$

where m_e is the mass of the electron. This defines the tendency of the plasma to oscillate due to a disturbance. The disturbance in our case was the electric field. In the presence of this electric field, the electrons, due to their light mass compared to ions, show excellent mobility and react immediately to the electric field where the ions remain static. This causes a charge separation causing polarization within the plasma. The polarization gives rise to internal electric field which tries to restore the charge neutrality. The electrons, because of the initial kinetic energy, gained move beyond their equilibrium position and the restoring force acts in the opposite direction of their motion and tries to bring them back to original position. The restoring force and electron motion causes what is known as plasma oscillations. In our simulation, we use λ_d and $1/\omega_p$ to normalize the space and time, respectively.

As explained, the plasma consists of electrons, ions, and neutral particles. Therefore, the system of fluid transport equation which describes the plasma properties is written separately for each particle. These equations are obtained by taking moments of the Boltzmann's equation. The first two moments represent the density and momentum. These equations are expressed in conservative form. The non-conservative form of expressing these equations was used by Ward *et al.* [8]. The first moment is given by the following equation

$$\frac{\partial n_k}{\partial t} + \nabla \cdot (n_k \vec{u}_k) = 0. \tag{1.3}$$

This is known as continuity equation describing the conservation of mass. The significance of each term can be explained by considering a small volume. First term represents the time

rate of change of the density of a particular species in a volume. Second term represents the difference between outflow and inflow flux of the particles inside the small volume. The second moment of the Boltzmann's equation gives rise to the momentum equation given by

$$\frac{\partial n_k \vec{u}_k}{\partial t} + \nabla \cdot (n_k \vec{u}_k \vec{u}_k) = -\frac{\nabla P_k}{m_k} + \frac{n_k}{m_k}\vec{F}. \tag{1.4}$$

On the left-hand side, the first term represents the time rate of change of a particle flux inside a small volume, and the second term represents the difference between outflow and inflow momentum flux of the particles. The first term on the right-hand side represents the force experienced due to pressure, and the last term represents any general force acting on the particles. The symbol n_k represents the density, $\vec{u}_k$ represents the velocity, m_k is the mass, and P_k is the pressure of the k^{th} species, respectively. $\vec{F}$ is the Lorentz force given by $\vec{F} = e(\vec{E} + \vec{u}_k \times \vec{B})$, where e is the charge of the ion or electron, $\vec{E}$ represents the electric field, and $\vec{B}$ is the magnetic field applied to the plasma. This is known as dyadic notation and is expanded below for a Cartesian coordinate system.

$$\begin{aligned} \vec{u}_k \vec{u}_k &= u_{kx}^2 \hat{x}\hat{x} + u_{kx}u_{ky}\hat{x}\hat{y} + u_{kx}u_{kz}\hat{x}\hat{z} \\ &\quad + u_{ky}u_{kx}\hat{y}\hat{x} + u_{ky}^2 \hat{y}\hat{y} + u_{ky}u_{kz}\hat{y}\hat{z} \\ &\quad + u_{kz}u_{kx}\hat{z}\hat{x} + u_{kz}u_{ky}\hat{z}\hat{y} + u_{kz}^2 \hat{z}\hat{z} \end{aligned} \tag{1.5}$$

So, the second term on the right-hand side of (1.4) can be written as

$$\begin{aligned} \nabla \cdot (n_k \vec{u}_k \vec{u}_k) &= \frac{\partial}{\partial x}\left(n_k u_{kx}^2 + n_k u_{ky}u_{kx} + n_k u_{kz}u_{kx}\right)\hat{x} \\ &\quad + \frac{\partial}{\partial y}\left(n_k u_{kx}u_{ky} + n_k u_{ky}^2 + n_k u_{kz}u_{ky}\right)\hat{y} \\ &\quad + \frac{\partial}{\partial z}\left(n_k u_{kx}u_{kz} + n_k u_{ky}u_{kz} + n_k u_{kz}^2\right)\hat{z}. \end{aligned} \tag{1.6}$$

The electrostatic potential ϕ in the plasma sheath region is governed by Poisson's equation given by

$$\nabla^2 \phi = \frac{e}{\epsilon_0}(n_i - n_e), \tag{1.7}$$

where n_i is the density of ions and n_e is the density of electrons. Equations (1.3), (1.4), and (1.7) together describe the evolution of plasma sheath in a space with respect to time.

The formation of sheath around a metal surface is the basic phenomenon observed in plasma [6]. The metal surface develops the negative potential with respect to plasma potential due to the absorption of the electrons. The ion and electron density is different in the sheath region. The potential in the sheath region increases from the negative potential on the metal surface to the plasma potential as we move from wall to the region where charge neutrality is maintained. This is simulated numerically in the case of 1D problem.

1.3 Analytical Approach

The analytical approach requires some assumptions so that the fluid equations described in previous section can be solved to provide an understanding of the plasma sheath. The equations can be solved in 1D, but becomes more difficult to solve in higher dimension where there are no closed forms of the solution. Since (1.4) is a nonlinear equation due to the presence of convective term, the solution to these equations cannot be solved analytically for plasma sheath without assuming the steady state. In steady state, the first term representing the time variation of the density or momentum is dropped. The analytical results can be summarized in the form of following equation [7]:

$$n_e = n_0 \ \exp\left(\frac{e\phi}{kT_e}\right), \tag{1.8}$$

where n_e is the electron density and T_e is the electron temperature in K. To obtain this, we solve the momentum equation for electrons and assume the electrons to be of zero mass compared to ions. The other assumptions which we make for the analytical solution to be valid are $T_i = T_e = T$ and $m_e u_e^2 \leq K_b T \leq m_i u_i^2$. We assume this relationship holds for the density of the electrons to find the numerical solution of the Poisson's equation. The ion density is given by

$$n_i = n_0 \ \exp\left(1 - \frac{2e\phi}{m_i u_{0i}}\right)^{-\frac{1}{2}}, \tag{1.9}$$

where m_i is the mass of ion and u_{0i} represents the ion velocity at the boundary where the charge neutrality is maintained. The expression for this velocity is given by

$$u_{0i} = \left(\frac{kT_i}{2\pi m_e}\right)^{1/2} \exp\left(\frac{e\phi_0}{kT_e}\right), \tag{1.10}$$

where ϕ_0 is the electric potential applied to the metal surface. The electric potential in the sheath region is given by

$$\phi = \phi_0 \ \exp\left(-\frac{x}{\chi}\right), \tag{1.11}$$

where χ being

$$\chi = \lambda_d^2 \left(1 - \frac{KT_i}{m_i u_{0i}^2}\right)^{-2}. \tag{1.12}$$

1.4 Numerical Approach

Since the formation of plasma sheath over a metal surface is governed by nonlinear behavior, it is difficult to solve it analytically for unsteady and higher-dimensional (more than one) cases. The numerical schemes can provide a great insight about the formation of sheath, describing both transient and steady state behavior. The different numerical approach depending upon the physics can be classified into either kinetic approach or the fluid approach. The kinetic approach requires the kinetic theory of gases, where the individual charge particle dynamics is followed inside a volume. This requires solving the Vlasov's equation [12] to get the distribution function which can then be used to find the velocity and spatial orientation of an individual charge particle. This approach is also known as Particle In Cell (PIC) simulation.

In the fluid approach, the collective behavior of the collection of particles is used and the plasma is treated using the fluid equations of continuity and momentum. This gives the density and velocity behavior of the particles as a collection. PIC simulations are generally used where wave particle interactions are of interest since fluid approach cannot by its own nature describe the single particle dynamics. Our simulation uses fluid approach because the ion density in the CubeSat's environment is high and tracking single particle dynamics

will require large computational resources.

The computational methods are effective to understand the physical phenomenons which are described by nonlinear partial differential equations, and the fluid transport equation to describe the plasma behavior is one of them. These methods are not an alternative to analytical or experimental way of understanding the physics, but a substitute. As a general approach, the problem of solving a physical system numerically consists of following steps [12].

- Define the partial differential equations describing the physical system.
- Discretize the equation, i.e. transforming the continuous models to difference equations so that they can be solved on a digital computer.
- Solve the difference equations thus obtained by defining the solution domain both in space and time. This also involves defining a grid over both space and time. If the solution of the difference equation depends only on the solution of previously calculated values it is known as explicit. If the solution also depends on the future values, then a system of linear algebraic equations are obtained and the method is known as implicit. The solution thus obtained is an approximate one.

The different approaches to solve these equations are finite-domain time differences and finite volume methods. In our approach, the finite volume method was used to solve for the evolution of sheath which is similar to that used by Chavelier *et al.* [13]. This approach differs from Ward *et al.* [8] where the nonlinear fluid equations were linearized in first order and the non-conservative form of fluid equations was used. Both approaches simulate the plasma fluid with initial drift velocity being zero, where as it is transonic in our 2D case.

1.5 Thesis Outline

Following the introduction, Chapter 2 defines the problem in 1D and explains the method to achieve numerical discretization. The chapter also discusses the necessary simulation parameters. The results obtained after running the simulation to steady state are

summarized using plots and compared with the analytical expressions. Chapter 3 also follows the same outline as that of Chapter 2. At the end of the chapter, the results are summarized using 2D plots. The conclusion of overall work and the future direction is discussed in Chapter 4.

Chapter 2

1D Study and Results

The plasma fluid equations given by (1.3) and (1.4) are reduced to 1D and are normalized both in space and time. The problem was solved in 1D to validate the numerical model against the known analytical expressions given in section 1.3. As explained in detail in the next section, the normalized equations are then discretized using the high order nonoscillatory central schemes. The Poisson's equation (1.7) was discretized using three node approximation and was solved nonlinearly using the conjugate gradient schemes. The difference equations obtained after discretization were coded into MATLAB^{TM} using the specified initial and boundary conditions on variables of interest (density, flux, and electric potential), and the simulation was run till the steady state was achieved and there was no variation in the variables. The simulation results showed a good match when compared with the analytical expressions.

The equation of continuity is given by

$$\frac{\partial n_i}{\partial t} + \frac{\partial n_i u_i}{\partial x} = 0. \tag{2.1}$$

The equation of momentum equation given by

$$\frac{\partial n_i u_i}{\partial t} + \frac{\partial n_i u_i^2}{\partial x} = -\frac{1}{m_i}\frac{\partial P_i}{\partial x} + \frac{n_i}{m_i}F, \tag{2.2}$$

where P_i is the pressure which is given by $n_i K_b T$. Since, we are considering only the electrostatic case. F is given by eE where E is the electric field given by$-e\frac{\partial \phi}{\partial x}$. The electric field is calculated from the nonlinear Poisson's equation using Boltzmann's relationship for

electrons. The equation is shown below:

$$\frac{\partial^2\phi}{\partial x^2} = \frac{e}{\epsilon_0}(n_i - n_0 \exp\left(\frac{e\phi}{kT_e}\right)). \tag{2.3}$$

The equations were normalized in space and time with λ_d and $1/\omega_p$, respectively. The density was normalized with the ambient ion density n_0 and the ion velocity with ion acoustic velocity given by $\sqrt{\frac{K_b T_i}{m_i}}$. The equations are then discretized both in space and time. Here the procedure to discretize the equations (2.1) and (2.2) would be described using central schemes and results would be compared with analytical expressions given in previous chapter.

2.1 Numerical Scheme

The fluid equations can be represented in the form of the following hyperbolic equation:

$$\frac{\partial u}{\partial t} + \frac{\partial f(u)}{\partial x} = \frac{\partial q(u)}{\partial x}. \tag{2.4}$$

In case of equation (2.1), we have $u = n_i$, $f(u) = n_i u_i$, and $q(u) = 0$. Similarly for equation (2.2) we have $u = n_i u_i$, $f(u) = n_i u_i^2 + \frac{1}{m_i} P_i$, and $q(u) = -e\phi$. The numerical solution is found by defining a uniform spatial and temporal grid where time is discretized using $t = n\Delta t$ where $n = (0, 1, 2 \ldots)$, $x = n\Delta x$, and $U_j^n = U(j\Delta x, n\Delta t)$. The fluid equations were discretized using the high-resolution central schemes [14] based on finite volume approach. The steps required to solve these equations using numerical difference equations are explained using the computational molecule shown in Fig. 2.1 in which the quantities used are defined by following equations:

$$\begin{aligned} H_{j+1/2}(t) &= \frac{F(u^+_{j+1/2}) + F(u^-_{j+1/2})}{2} \\ &\quad - \frac{a_{j+1/2}}{2}(u^+_{j+1/2} - u^-_{j+1/2}), \end{aligned} \tag{2.5}$$

$$P_{j+1/2}(t) = \frac{Q(u_j) + Q(u_{j+1})}{2}, \tag{2.6}$$

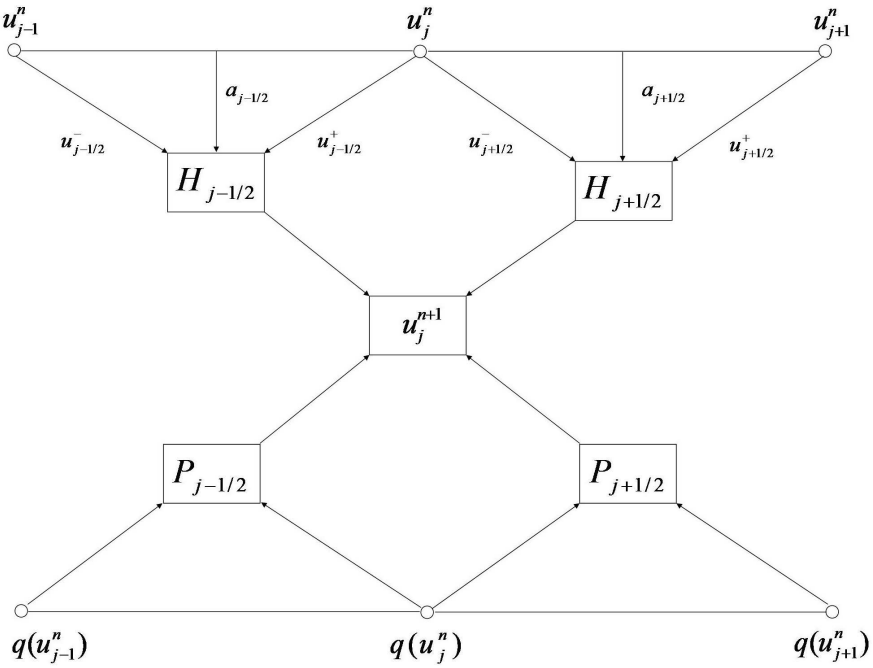

Fig. 2.1: Numerical scheme for fluid equations in 1D.

where $a_{j+1/2}$ is the local speed in each cell. The quantities are given by

$$u^{\pm}_{j+1/2} = u_{j+1} \mp \frac{\Delta x}{2}(u_x)_{j+1/2\mp 1/2}, \tag{2.7}$$

where u_x is given by

$$(u_x)^n_j = \text{minmod}\left(\frac{u^n_j - u^{n-1}_j}{\Delta x}, \frac{u^{n+1}_j - u^n_j}{\Delta x}\right), \tag{2.8}$$

and minmod limiter is defined as $\text{minmod}(a,b) = \frac{1}{2}[\text{sgn}(a) + \text{sgn}(b)].\min(|a|, |b|)$. The final difference equations are defined using the following equation:

$$\begin{aligned} \frac{du_j}{dt} &= -\frac{H_{j+1/2} - H_{j-1/2}}{\Delta x} \\ &\quad + \frac{P_{j+1/2} - P_{j-1/2}}{\Delta x}. \end{aligned} \tag{2.9}$$

The Euler scheme is used to the march this equation forward in time. The time step Δt varies according to the Courant Friedrichs Lewy (CFL) condition given by

$$\Delta t = C/\max\left(\frac{a_{j+1/2}}{\Delta x}\right), \tag{2.10}$$

where C is the Courant number and is set to 1/8 in our simulations.

The equation (2.3) has a nonlinear term due to presence of Boltzmann's relation for electron density. The computational scheme for the same is shown in Fig. 2.2. It can be represented in the form of the function of ϕ given by

$$h(\phi) = \frac{\phi_{i+1} - 2\phi_i + \phi_{i-1}}{\Delta x^2} + \frac{e}{\epsilon_0}(n_i - n_0\ exp\left(\frac{e\phi}{kT_e}\right)). \tag{2.11}$$

This equation is solved iteratively, where ϕ_k represents the value in the kth iteration. So for the next iteration, the ϕ_{k+1} can be found using the Taylor series expansion and neglecting the higher order terms

$$h(\phi^{k+1}) = h(\phi^k) + h'(\phi^k)(\phi^{k+1} - \phi^k) = 0, \tag{2.12}$$

$$\delta^k = (\phi^{k+1} - \phi^k), \tag{2.13}$$

which reduces to

$$h'(\phi^k)\delta^k = h(\phi^k), \tag{2.14}$$

which is in the form of linear system of algebraic equations $AX = B$. The A is found by Jacobian matrix given by

$$A_{mn} = \begin{matrix} 1/\Delta x^2 & m = i,\ n = i \pm 1 \\ -\frac{2}{\Delta x^2} - \frac{n_0 e^2}{kT_e \epsilon} exp\left(\frac{e(\phi - \phi_0)}{kT_e}\right) & m = n = i. \end{matrix} \tag{2.15}$$

In each iteration, a linear system of equations is to be solved to obtain the value for δ_k.

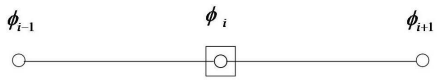

Fig. 2.2: Numerical scheme for Poisson's equation in 1D.

This value is then added to ϕ_k to obtain new value for ϕ at each spatial node, which is then used in next iteration. Since the A matrix is sparse, the biconjugate gradient scheme [15] is used to solve the linear system of equations. For each iteration, the tolerance level for RMS error is set to 10^{-7}. This method seems to converge if the initial guess is sufficiently close to the solution.

2.2 Simulation Parameters

The length, density, velocity, and time were normalized using electron Debye length, average ion density, acoustic speed of the ions and plasma period (calculated from plasma frequency), respectively. The simulation parameters for other quantities are summarized as:

Density n_0: 1,

Electron temperature: 0.1 eV,

Ion temperature: 0.1 eV,

Plasma potential: 0 V,

Potential applied at the metal surface: -0.2 V.

The electric potential was chosen to be -0.2 V because of two reasons. First, when a negative voltage is applied to the metal surface a stable plasma sheath is formed. Secondly, to compare the results for analytical expressions of the ion density and electric potential the potential on the metal wall should be comparable to the electron temperature. The computational domain was of length $L = 50\lambda_d$. The small space step Δx was chosen to be 0.2. The infinite metal wall was place at the left boundary and the inflow of the particles was at the right boundary. The model of the system was made to evolve with the time.

The initial conditions were

$$n_i(x,0) = 1; u_{ix}(x,0) = 0. \tag{2.16}$$

The boundary conditions for the domain were

$$n_i(L,t) = 1;\ \phi(0,t) = -0.2;\ \phi(L,t) = 0. \tag{2.17}$$

The u_i at the boundary cell were calculated using the extrapolation depending upon the two neighboring cells.

2.3 Results

The simulation was run using MATLAB^{TM} on Windows Environment using Dual Core AMD Opteron Processor 165 (1.81GHz). The RAM memory required for the simulation domain was 50MB. The obtained results for ion density and electron potential were compared with the analytical expressions given in section 1.3. The time taken for one plasma period to complete was 5 seconds. The results of the 1D problem obtained after running the simulation for 3500 plasma periods are summarized in Fig. 2.3 to Fig. 2.9. During the initial stage, when the sheath was forming there were waves observed travelling from the sheath region to the inflow boundary. The amplitude of these waves eventually subsides when the steady state is achieved.

Figure 2.3 shows the final ion density and electron density. The ion density was obtained by solving the plasma fluid equations numerically. The electric potential obtained from Poisson's equation was substituted in the Boltzmann's relationship for electrons to get the electron density. As can be seen, the result shows the formation of plasma sheath for the applied negative electric potential. The ions and electrons arrange themselves around the metal wall in order to create an electric field which opposes the electric field due to the metal wall. The metal wall surface due to its negative electric potential tends to absorb the ions and cause a slump in the ion density. Now electrons with ions are forced towards the metal surface to maintain the charge neutrality of plasma, but because of the higher

mobility are removed from the region at a faster rate than the ions. This causes more decrease in the electron density as compared to the ion density. The plasma sheath thus formed has a thickness of 8 λ_d. The electrons start decreasing from the equilibrium ion density at around 8 λ_d and the ions start at 5 λ_d.

The comparison of ion density for the simulation and analytical approach is done in Fig. 2.4. The ion density matches perfectly in the region where the charge neutrality is maintained. In the sheath region there is slight decrease in the ion density for simulated results. This decrease is due to the assumptions which were made in deriving the analytical expression for the density. In the analytical approach, the ions were assumed to be cold so the pressure was not taken into account. In numerical approach, the pressure contributed to the diffusion of the ions towards the metal wall.

In Fig. 2.5, we have compared the electric potential. The electric potential is equal to the plasma potential in the nonsheath region and in the sheath region it begins to drop to the value of the applied potential the metal surface. The electric potential shows a good match compared to the ion density for the simulated results. This is because we are using the difference of the ion and electron density on a small space interval for calculating the electric potential, of which the electron density uses the analytical expression.

The simulation started with the ions having zero velocity. When the steady state is achieved, the sheath formed, in Fig. 2.6 we see the ion velocity to be at Bohm's Velocity at inflow boundary and gradually increase in the sheath region to the value of 1.46 times the thermal velocity at the metal surface. The negative value of the ions here is due to the ions moving in negative direction. The plots showed a similar results what was observed in the work of Chavelier *et al.* [13] and confirmed the validity of the scheme to simulate the time evolution of plasma sheath over a metal surface.

Figure 2.7 to Fig. 2.9 show the simulation for the variation as we keep on increasing the negative electric potential on the metal surface of the CubeSat. The variation of ion density with electric potential is shown in Fig. 2.7. Figure 2.8 shows the variation of corresponding electric potentials. As we see in Fig. 2.9, the ions are removed at faster rate when the

applied negative potential is increased and therefore the slump in the ion density in Fig. 2.7 increases.

As can be seen from Fig. 2.4 and Fig. 2.5, the numerical results showed a good and reasonable agreement with the analytical expressions. This validates our numerical approach and the same is applied to the 2D case.

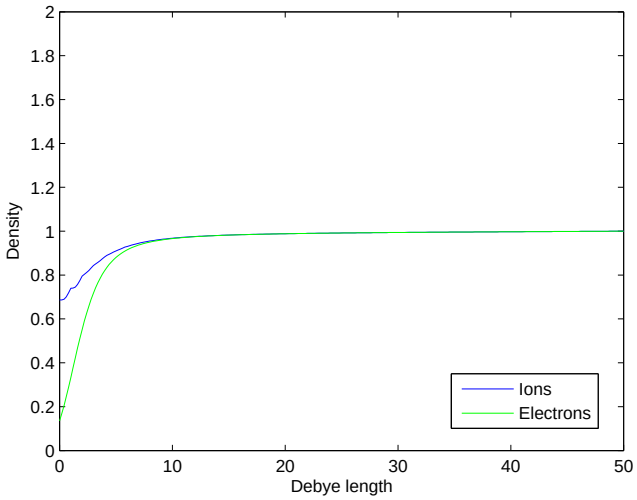

Fig. 2.3: Plasma sheath.

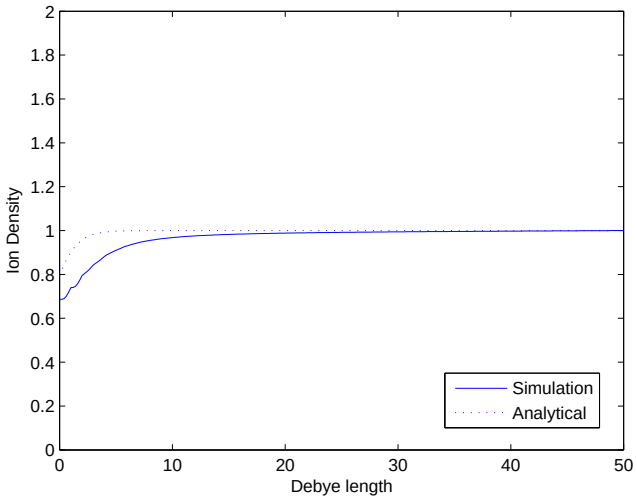

Fig. 2.4: Normalised ion density in 1D.

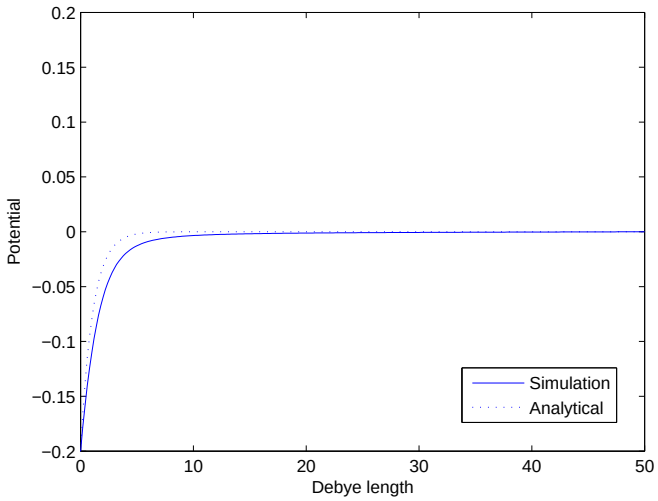

Fig. 2.5: Electric potential (Volts) in 1D.

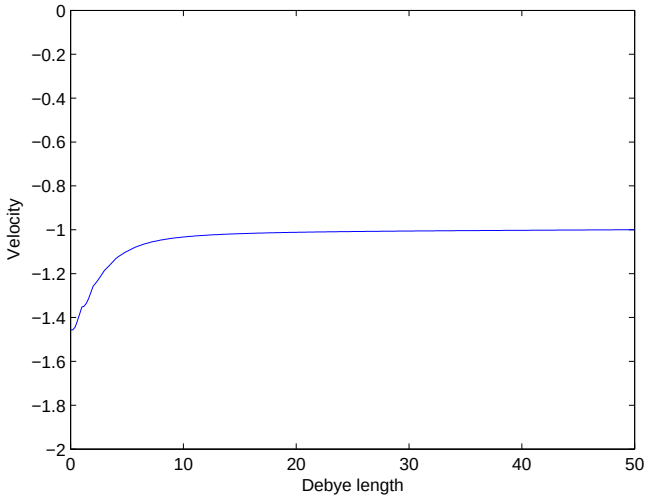

Fig. 2.6: Normalised ion velocity in 1D.

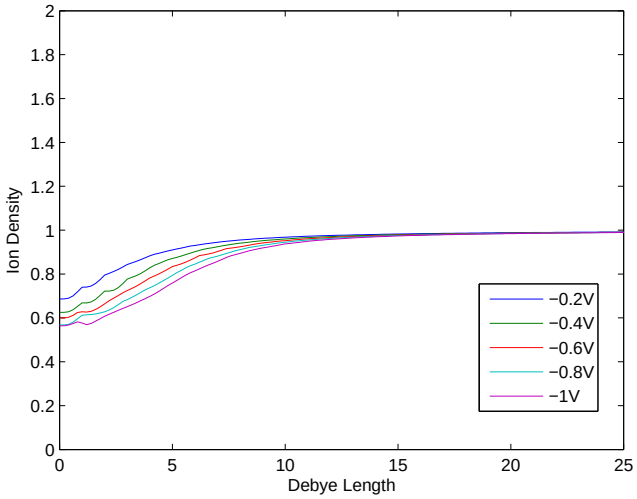

Fig. 2.7: Ion density curves.

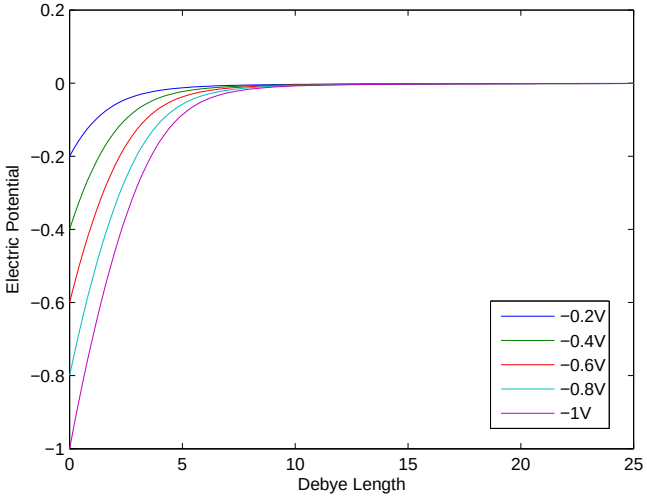

Fig. 2.8: Electric potential curves.

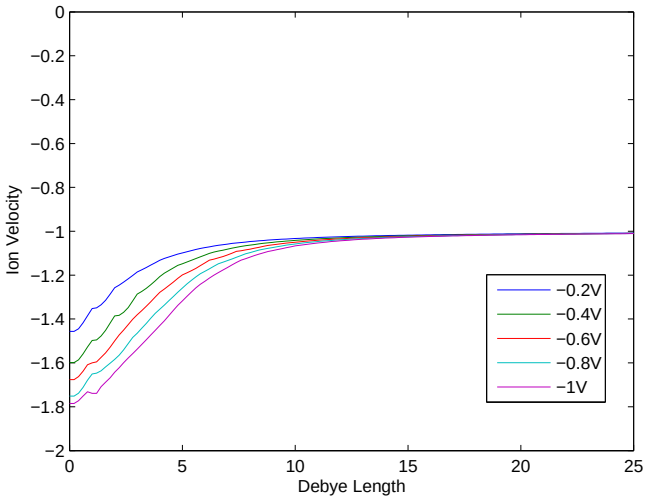

Fig. 2.9: Velocity curves.

Chapter 3

2D Study and Results

In 2D, we extend the problem which was done in 1D. The difference here is adding one extra dimension introduces one more term for flux in the fluid equations. The objective here is to study the dynamics of plasma around the CubeSat model. The variation of plasma quantities is considered along x and y direction. The momentum equation representing the motion of the ions is defined for both the directions. The process of extending to 2D follows from the 2D fluid equations and the Poisson's equation derived from the previously defined equations (1.3), (1.4), and (1.7). Then we discretize these using the same schemes which we used in 1D and validity of which was proved in the obtained simulation results. After discretizing, the numerical difference equations were simulated using a given set of parameters for two different directions of ion flux. The simulation was run long enough to achieve the steady state showing the time evolution of wake structure around the CubeSat.

If we consider the evolution of the sheath in 2D, i.e. the variation of the quantities in the x and y direction, then the equation for continuity is

$$\frac{\partial n_i}{\partial t} + \frac{\partial (n_i u_{ix})}{\partial x} + \frac{\partial (n_k u_{iy})}{\partial y} = 0. \tag{3.1}$$

Accordingly, the equation of momentum reduces to

$$\frac{\partial n_i u_{ix}}{\partial t} + \frac{\partial (n_i u_{ix}^2)}{\partial x} + \frac{\partial (n_i u_{ix} u_{iy})}{\partial y} = -\frac{1}{m_i}\frac{\partial P_i}{\partial x} + \frac{n_i}{m_i} F_x, \tag{3.2}$$

$$\frac{\partial n_i u_{iy}}{\partial t} + \frac{\partial (n_i u_{ix} u_{iy})}{\partial x} + \frac{\partial (n_i u_{iy}^2)}{\partial y} = -\frac{1}{m_i}\frac{\partial P_i}{\partial y} + \frac{n_i}{m_i} F_y, \tag{3.3}$$

where $F_x = -e\frac{\partial \phi}{\partial x} + u_{iy} B_x$ and $F_y = -e\frac{\partial \phi}{\partial y} + u_{ix} B_y$ is the force due to electrostatic field and

the pressure term is given by $P_i = n_i K_b T$. In our case, since we consider the unmagnetized plasma we drop the magnetic field in the force term.

The Poisson's equation in 2D is

$$\frac{\partial^2 \phi}{\partial x^2} + \frac{\partial^2 \phi}{\partial y^2} = \frac{e}{\epsilon_0}\left(n_i - n_0 \exp\left(\frac{e\phi}{kT_e}\right)\right). \tag{3.4}$$

There is no analytical solution to these equations in higher dimension, so the only way they can be solved is numerically which is described in next section.

3.1 Numerical Scheme

The numerical solution is found by discretizing the fluid equations using the same high-resolution central schemes based on finite volume approach as was done for 1D. The fluid equations can be represented in the form of following hyperbolic equation:

$$\frac{\partial u}{\partial t} + \frac{\partial f(u)}{\partial x} + \frac{\partial g(u)}{\partial y} = \frac{\partial q(u)}{\partial x} + \frac{\partial q(u)}{\partial y}. \tag{3.5}$$

In case of equation (3.1), we have $u = n_i$, $f(u) = n_i u_{ix}$, $g(u) = n_i u_{iy}$, and $q(u) = 0$. Similarly for equation (3.2), we have $u = n_i u_{ix}$, $f(u) = n_i u_{ix}^2 + \frac{1}{m_i} P_i$, $g(u) = n_i u_{ix} u_{iy}$, and $q(u) = -e\phi$, but the second source term would be dropped because there is no variation of electric field in y- direction for this equation. The equation (3.3) will have $u = n_i u_{iy}$, $f(u) = n_i u_{ix} u_{iy}$, $g(u) = n_i u_{iy}^2 + \frac{1}{m_i} P_i$, and $q(u) = -e\phi$; in this case the first source term would be dropped. The scheme consists of three basic steps shown pictorially in Fig. 3.1 to Fig. 3.3 and mathematically in the following equations:

$$\begin{aligned} \frac{du_{j,k}}{dt} &= -\frac{H^x_{j+1/2,k} - H^x_{j-1/2,k}}{\Delta x} - \frac{H^y_{j,k+1/2} - H^y_{j,k-1/2}}{\Delta y} \\ &\quad + \frac{P^x_{j+1/2,k} - P^x_{j-1/2,k}}{\Delta x} + \frac{P^y_{j,k+1/2} - P^y_{j,k-1/2}}{\Delta y}, \end{aligned} \tag{3.6}$$

$$H^x_{j+1/2,k}(t) = \frac{F(u^+_{j+1/2,k}) + F(u^-_{j+1/2,k})}{2} - \frac{a^x_{j+1/2,k}}{2}(u^+_{j+1/2,k} - u^-_{j+1/2,k}), \tag{3.7}$$

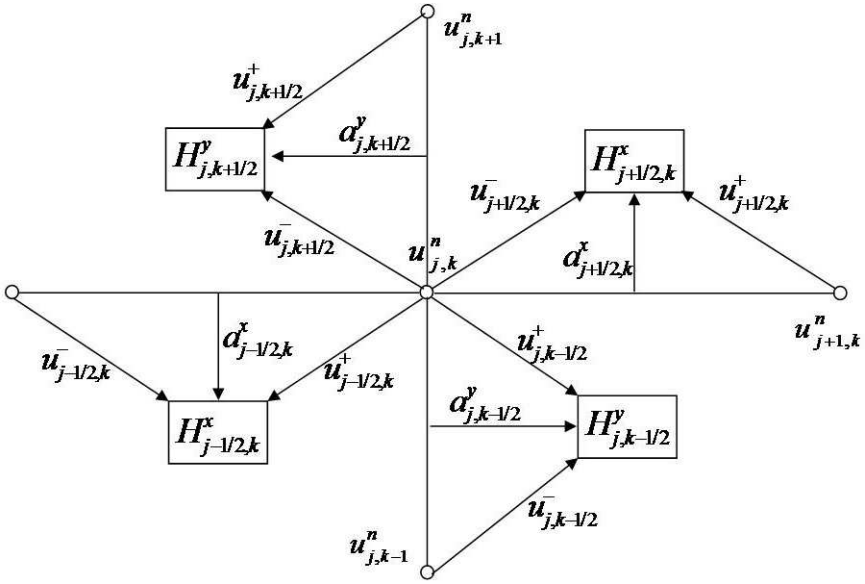

Fig. 3.1: Numerical scheme for fluid equation Step 1.

$$H^y_{j,k+1/2}(t) = \frac{G(u^+_{j,k+1/2}) + G(u^-_{j,k+1/2})}{2} - \frac{a^y_{j,k+1/2}}{2}(u^+_{j,k+1/2} - u^-_{j,k+1/2}), \tag{3.8}$$

$$P^x_{j+1/2,k}(t) = \frac{Q(u_{j,k}) + Q(u_{j+1,k})}{2}, \tag{3.9}$$

$$P^y_{j,k+1/2}(t) = \frac{Q(u_{j,k}) + Q(u_{j,k+1})}{2}, \tag{3.10}$$

where $a^x_{j+1/2,k}$ and $a^y_{j,k+1/2}$ are the local speed in x and y directions, respectively, for each cell. The quantities are given by

$$u^\pm_{j+1/2,k} = u_{j+1,k} \mp \frac{\Delta x}{2}(u_x)_{j+1/2\mp 1/2,k}, \tag{3.11}$$

$$u^\pm_{j,k+1/2} = u_{j,k+1} \mp \frac{\Delta y}{2}(u_y)_{j,k+1/2\mp 1/2}. \tag{3.12}$$

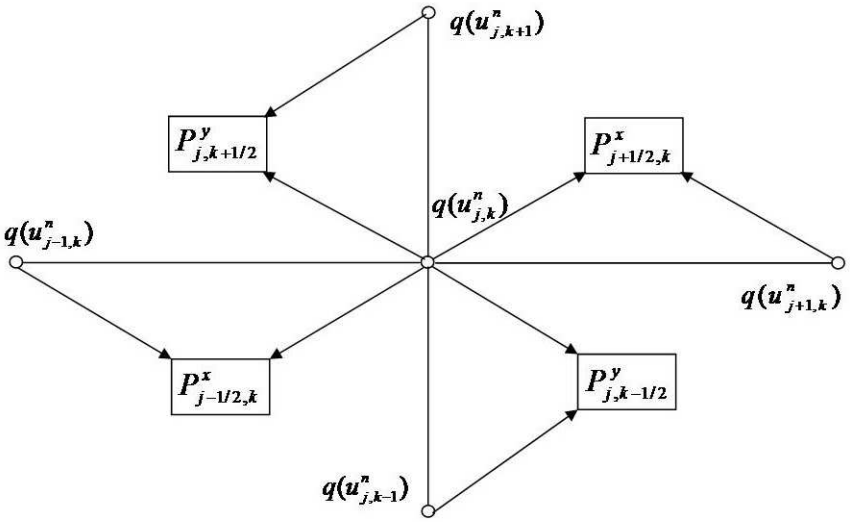

Fig. 3.2: Numerical scheme for fluid equation Step 2.

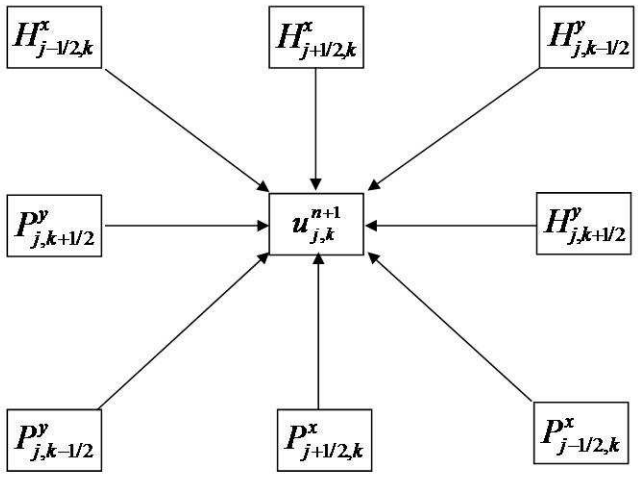

Fig. 3.3: Numerical scheme for fluid equation Step 3.

The Euler scheme is used to march the equation (3.6) forward in time. The time step varies according to the CFL condition given by

$$\Delta t = C/\max\left(\frac{a^x_{j+1/2,k}}{\Delta x}\ \frac{a^y_{j,k+1/2}}{\Delta y}\right), \tag{3.13}$$

where C is set to 1/8 for the simulation.

Equation (3.4) can be represented in the form of the function of ϕ given by

$$\begin{aligned} h(\phi) &= \frac{\phi_{i+1,j} - 2\phi_{i,j} + \phi_{i-1,j}}{\Delta x^2} + \frac{\phi_{i,j+1} - 2\phi_{i,j} + \phi_{i,j-1}}{\Delta y^2} \\ &\quad + \frac{e}{\epsilon_0}\left(n_i - n_0 \exp\left(\frac{e\phi}{kT_e}\right)\right), \end{aligned} \tag{3.14}$$

where n_e is replaced with the expression for Boltzmann's relation for electrons given by equation (1.8).

As given in the 1D case, the form of linear system of algebraic equations $AX = B$. The computational molecule for the same is given in Fig. 3.4. Now if we have N_x grid points along x-axis and N_y along y-axis, we get $i = 1$ to N_x and $j = 1$ to N_y. Let us define the current node for calculating the sparse matrix as $N_c = i + (j-1)N_x$. Matrix A is found by Jacobian matrix $h'(\phi^k)$ given by

$$A_{mn} = \begin{cases} 1/\Delta x^2 & m = i,\ n = N_c \pm 1 \\ 1/\Delta y^2 & m = i,\ n = N_c \pm N_x \\ -\frac{2}{\Delta x^2} - \frac{2}{\Delta y^2} - \frac{n_0 e}{kT_e \epsilon} \exp\left(\frac{\phi - \phi_0}{kT_e}\right) & m = n = N_c. \end{cases} \tag{3.15}$$

The tolerance level for the RMS error was decided as 10^{-7}.

3.2 Simulation Parameters

The simulation parameters were same as that in the 1D case. The only difference here is the computational domain has an extra dimension. The solution domain for the difference

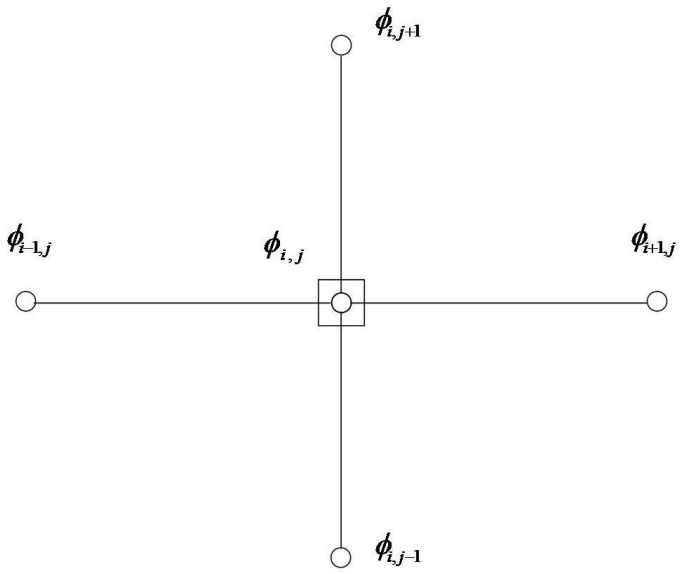

Fig. 3.4: Numerical scheme for Poisson's equation in 2D.

equation was confined along the x-axis and y-axis over a region of an area $L_x \times L_y$. Since the boundary for the solution of the plasma fluid equations (3.1), (3.2), (3.3), and (3.4) exists at infinity, to solve the difference equations (3.6) and (3.14) the boundary needs to be at some finite value. In the case of ion flux entering the domain at an angle of 45 degrees, the boundary was chosen to be at $L_x = L_y = 100\lambda_d$. The number of grid points per λ was chosen to be 2. So, the value for Δx is $0.5\lambda_d$. The metal cube of width 5 λ_d was placed at (25,25) from the origin of the computational domain. For the second case where the ion flux is parallel to x-axis, the x and y-boundary were at $L_x = 70\lambda_d$ and $L_y = 150\lambda_d$, respectively. The metal cube was placed at (25,75). The value for L_x and L_y were chosen such that they were sufficiently large compared to the size of the metal cube, and sufficiently small compared to the use of the collisionless plasma model. Since Boltzmann's relationship for the electron density was used, the mass of the ions was that of the realistic model. The temperature of ions was equal to that of electrons. The density and velocity at inflow boundaries were fixed on the initial values, whereas at outflow boundaries of the metal

surface and the computational domain were calculated using the first order extrapolation using the interior cells. The electric potential was specified on the metal surface and was extrapolated on the boundaries of computational domain using the linear extrapolation. The initial condition for the case where the ion flux is 45 degrees to x-axis is given by

$$n_i(x, y, 0) = 1;\ u_{ix}(x, y, 0) = 1.77;\ u_{iy}(x, y, 0) = 1.77, \tag{3.16}$$

and for the case where it is parallel to x-axis is

$$n_i(x, y, 0) = 1;\ u_{ix}(x, y, 0) = 2.5;\ u_{iy}(x, y, 0) = 0. \tag{3.17}$$

3.3 Results

The RAM memory required for the simulation domain 450MB. The time taken for one plasma period to complete was 3.5 hours. The simulation was run for 299.51 plasma periods. The density profile showed no change after 50 plasma periods, so compared to 1D simulation the steady state was achieved sooner. The simulation for the case where ion flux was parallel to x-axis took more time steps for a single plasma period because of the CFL condition requirement.

The density profile starts with single tail in the rarefaction region which divides into two. The profile shows symmetric behavior around the ion flux direction. The wake structure expands both in the direction perpendicular and parallel to the ion flux direction. After running the simulation for 299.51 plasma periods, we obtain the initial density profile shown in Fig. 3.5 and Fig. 3.6 where we see the rarefaction waves at the front and back of the metal cube. In this region, the ion density varies from 0.56 to 0.8. There was a small density build up near the CubeSat's rear end. This was because as we move from the CubeSat's rear surface towards the outflow boundary we experience the ions reversing there direction of momentum.

Figure 3.7 and Fig. 3.8 shows the electric potential profile. The electric potential because of nonlinear Poisson's equation mimics the behavior of the ion density. The electric

potential in the rarefaction region was found to be varying between -0.001 to -0.04V approximately for both the case. The region behind the CubeSat was showing an electric potential of -2×10^{-4}V and -8×10^{-4}V for the first case and second case, respectively.

The ion flux in along the x-axis is shown in Fig. 3.9 and Fig. 3.10, and along y-axis is shown in Fig. 3.11 and Fig. 3.12. For the first case, the ion flux along x axis, we see that the ions in the rarefaction region develop the velocity which varies from 0.2 to 0.4 magnitude where as for ion flux along y-axis shows a symmetric structure varies from 1.2 to 2. For the second case, we see the ion flux along y-axis and x-axis seems to mirror the structure along the direction of ion flux. The value of the flux tends to reduce behind the CubeSat for both the axis.

The magnitude of the velocity of ions is shown in Fig. 3.13 and Fig. 3.14. As can be seen, in the rarefaction region we see the magnitude has increased than the initial ion velocity and has decreased in the region behind the Cubesat. In the density build up region, we see that the magnitude of the ion velocity decreases significantly compared to the other regions of the wake structure. Figure 3.15 and Fig. 3.16 show the vector diagram for the trajectory of ions near the CubeSat Surface. Here the ions reverse their direction of motion. Using the plasma fluid equations, the results shows that there is formation of plasma wake structure around the CubeSat and the ion density and the motion is affected because of the applied electric potential.

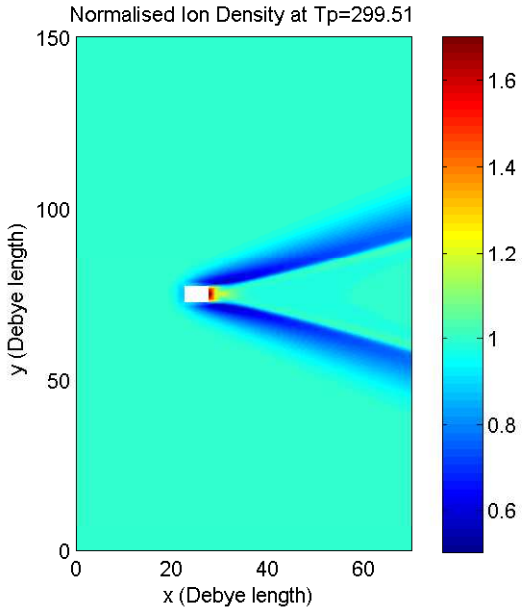

Fig. 3.5: Normalised density for ions entering parallel to x-axis.

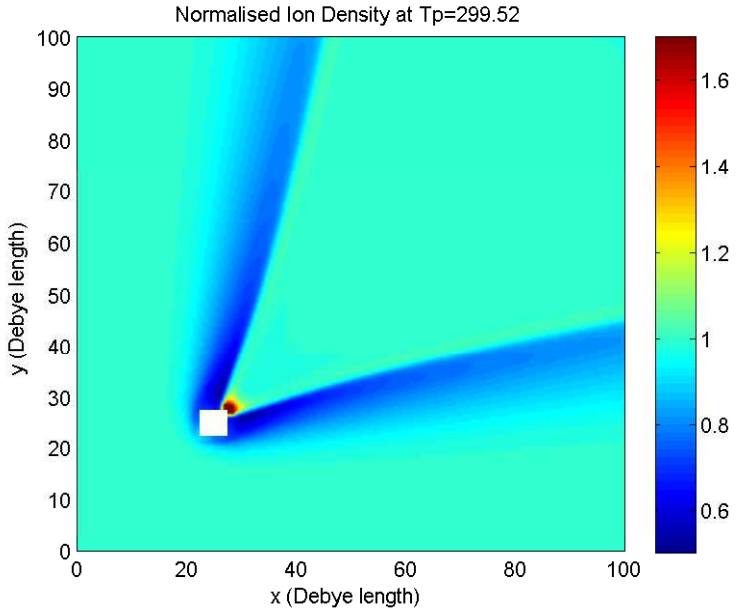

Fig. 3.6: Normalised density for ions entering at 45 degrees to x-axis.

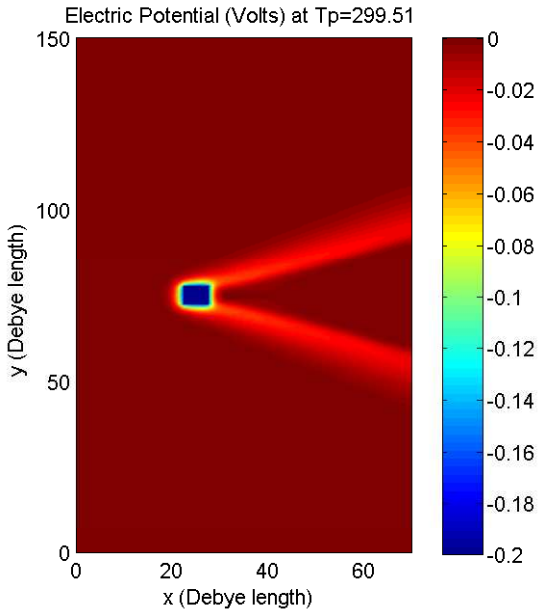

Fig. 3.7: Electric potential (Volts) for ions entering parallel to x-axis.

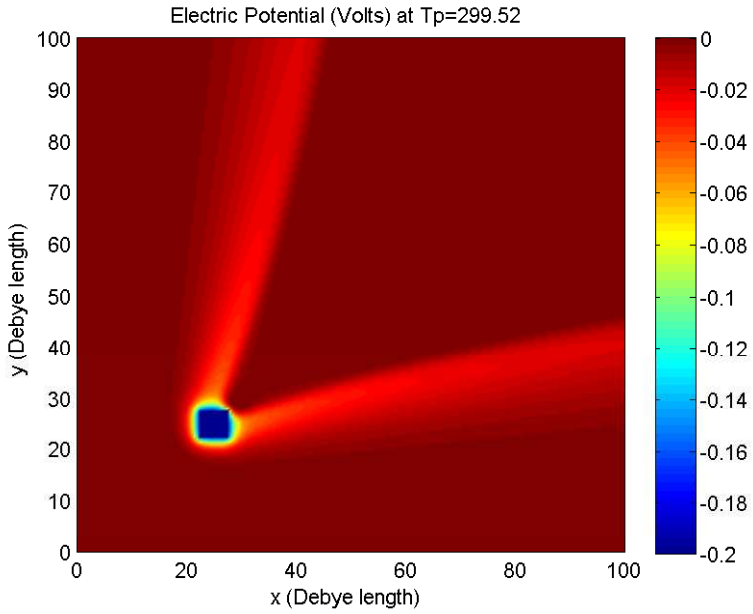

Fig. 3.8: Electric potential (Volts) for ions entering at 45 degrees to x-axis.

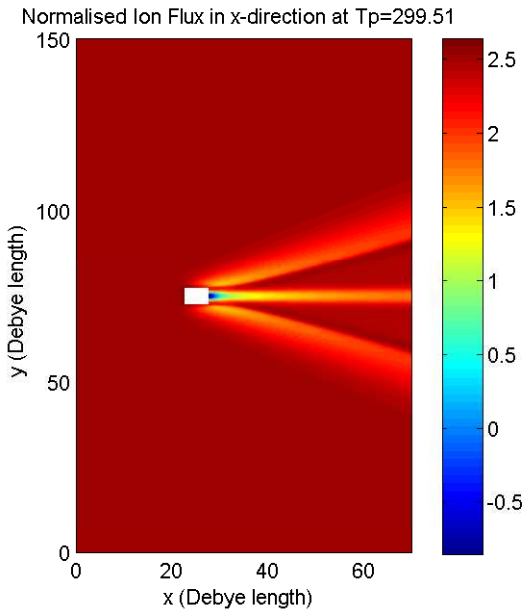

Fig. 3.9: Normalized flux along x-axis for ions entering parallel to x-axis.

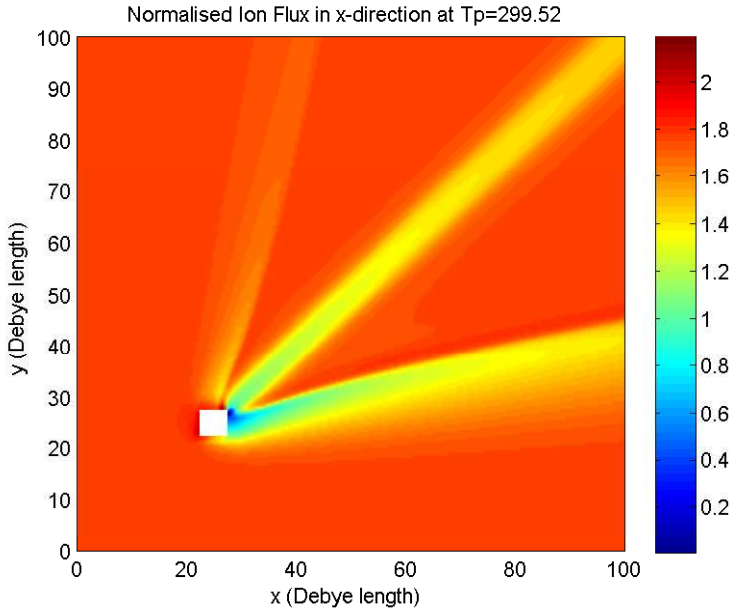

Fig. 3.10: Normalized flux along x-axis for ions entering at 45 degrees to x-axis.

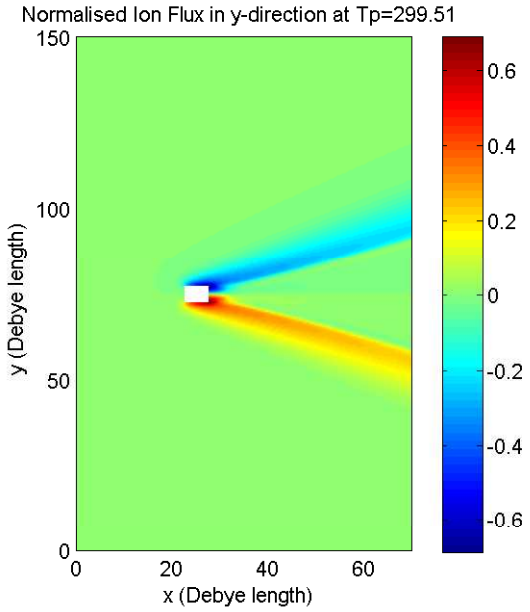

Fig. 3.11: Normalized flux along x-axis for ions entering parallel to x-axis.

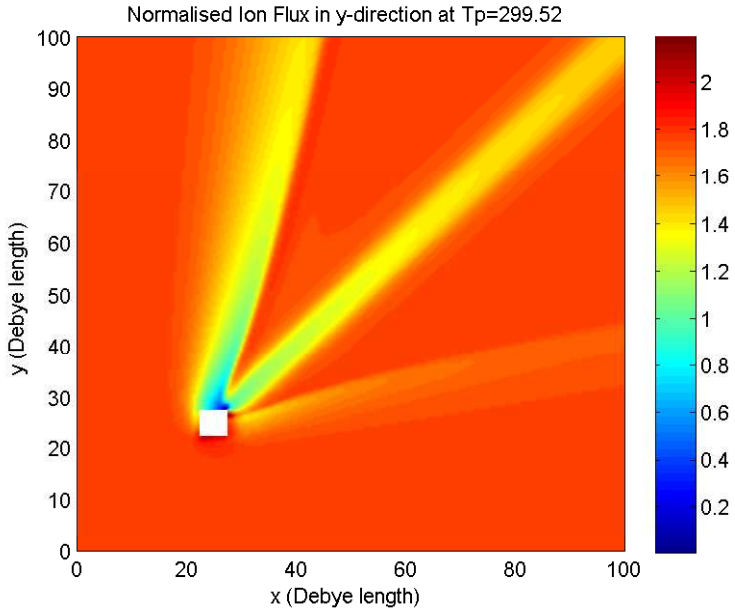

Fig. 3.12: Normalized flux along x-axis for ions entering at 45 degrees to x-axis.

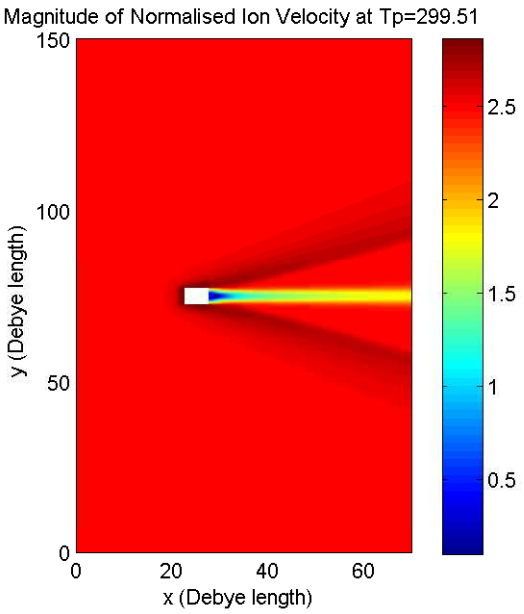

Fig. 3.13: Magnitude of normalized velocity for ions entering parallel to x-axis.

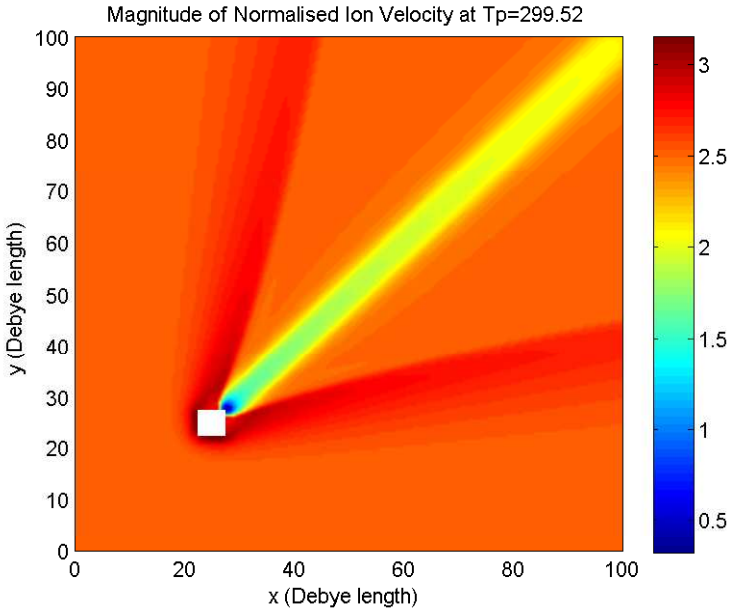

Fig. 3.14: Magnitude of normalized velocity for ions entering at 45 degrees to x-axis.

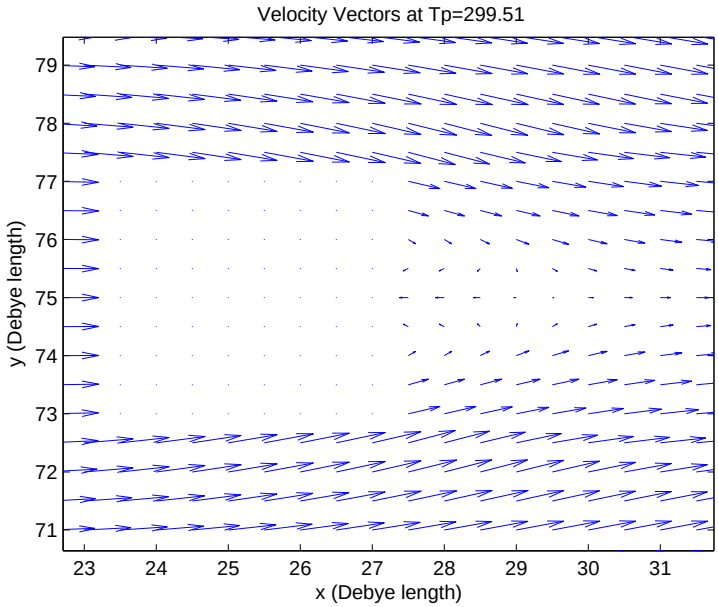

Fig. 3.15: Velocity vectors for ions entering parallel to x-axis.

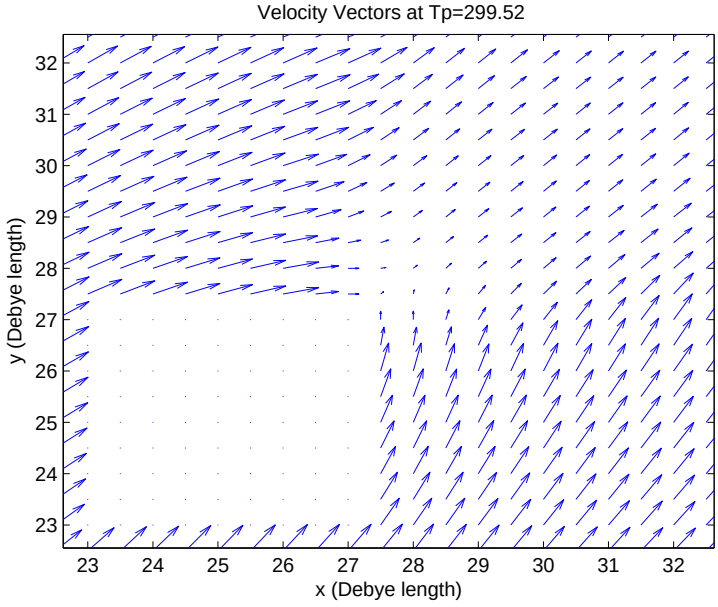

Fig. 3.16: Velocity vectors for ions entering at 45 degrees to x-axis.

Chapter 4

Conclusion

The numerical scheme used to solve the fluid equation was able to simulate the wake structure around the CubeSat. The validity of scheme was tested using the application to 1D problem and comparing it with the analytical expressions. The comparison shows a good match with the plots of simulated results and the analytical expression.

In 2D simulation, the simulation time required for one plasma period seemed to be decreasing with the increase in the angle at which ions entered inside the computational domain. This was due to the CFL condition which depends on ion velocity both in x and y directions. The ion density and electric potential shows the symmetric structure around the ion flux direction. The ion density shows the formation of rarefaction waves, in this region the electric potential is positive with respect to CubeSat and negative with respect to plasma potential.

In the simulation results, a unphysical density build up was seen as shown in Fig. 3.5 and 3.6. These density build up shows that the fluid apporach cannot simulate the collisionless plasma model. As can be seen in Fig. 3.15 and Fig. 3.16, the place where the wake closes we see this density buildup. In a collisionless model, the trajectories of the ions should cross each other. The inherent nature of the fluid schemes causes the flux being averaged in this closing cell. This causes the flow of the fluid in this merging cell which eventually causes the density buildup. The solution to overcome this density build up is to develop hybrid schemes which simulates the wake structure near the CubeSat using particle-in-cell approach and using fluid approach for the plasma in the far region.

In future, the same simulation can be run to study the effect of a magnetic field on the ion density and momentum. The plasma simulations can be extended to multiple species and neutral atoms. The effect of the same on the plasma environment of the CubeSat can

be studied. The scheme can be extended to complex 3D environment to simulate the real scenarios using time varying electric and magnetic fields.

References

[1] R. Munakata, "Cubesat design specification rev. 12," The CubeSat Program, California Polytechnic State University, 2009.

[2] J. Brown, "Test pod user's guide," The CubeSat Program, California Polytechnic State University, 2000.

[3] A. Toorian, E. Blundell, J. Puig-Suari, and R. Twiggs, "Cubesats as responsive satellites," in *Space Conference, American Institute of Aeronautics and Astronautics*, Aug. 2005.

[4] M. N. Mahmoud, "Integrated solar panel antennas for cube satellites," Master's thesis, Utah State University, Logan, UT, 2010.

[5] A. Toorian, K. Diaz, and S. L. , "The cubesat approach to space access," in *Aerospace Conference, 2008 IEEE*, pp. 1–14, Mar. 2008.

[6] K. U. Riemann, "Residual vector quantizers with jointly optimized code books," *Journal of Physics*, vol. 24, pp. 493–518, 1991.

[7] J. A. Bittencourt, *Fundamentals of Plasma Physics*. New York: Springer, 2004.

[8] J. Ward, C. Swenson, and C. Furse, "The impedance of a short dipole antenna in a magnetized plasma via a finite difference time domain model," *Antennas and Propagation, IEEE Transactions on*, vol. 53, no. 8, pp. 2711–2718, Aug. 2005.

[9] E. Grossman and I. Gouzman, "Space environment effects on polymers in low earth orbit," *Nuclear Instruments and Methods in Physics Research Section B: Beam Interactions with Materials and Atoms*, vol. 208, pp. 48–57, 2003.

[10] R. A. Heelis, "Electrodynamics in the low and middle latitude ionosphere: a tutorial," *Journal of Atmospheric and Solar-Terrestrial Physics*, vol. 66, no. 10, pp. 852–838, 2004.

[11] P. M. Banks, "Thermal conduction and ion temperatures in the ionosphere," *Earth and Planetary Science Letters*, vol. 1, no. 5, pp. 270–275, 1966.

[12] E. Halickova, "Fluid model of plasma and computational methods for solution," in *Week of Doctoral Students 06 Proceedings of Contributed Papers: Part III*, pp. 180–186, 2006.

[13] T. W. Chavelier, U. S. Inan, and T. F. Bell, "Fluid simulation of the collisionless plasma sheath surrounding an electric dipole antenna in the inner magnetosphere," *Radio Science*, vol. 45, RS1010, p. 18, 2010.

[14] A. Kurgnov and E. Tadmor, "New high-resolution central schemes for nonlinear conservation laws and convection-diffusion equations," *Journal of Computational Physics*, pp. 241–246, 2000.

[15] R. J. Leveque, *Finite Difference Methods for Ordinary and Partial Differential Equations: Steady-State and Time-Dependent Problems.* Philadelphia: SIAM, 2007.